Non-invasive determination of gas phase dispersion coefficients in bubble columns using periodic gas flow modulation

Döß, A.; Schubert, M.; Bieberle, A.; Hampel, U.;

Originally published:

May 2017

Chemical Engineering Science 171(2017), 256-270

DOI: https://doi.org/10.1016/j.ces.2017.05.019

Perma-Link to Publication Repository of HZDR:

https://www.hzdr.de/publications/Publ-25198

Non-invasive determination of gas phase dispersion coefficients in bubble columns using periodic gas flow modulation

Alexander Döß[1], Markus Schubert[1], André Bieberle[1], Uwe Hampel[1,2]

[1] Institute of Fluid Dynamics, Helmholtz-Zentrum Dresden-Rossendorf, Bautzner Landstr. 400, 01328 Dresden, Germany.

[2] AREVA Endowed Chair of Imaging Techniques in Energy and Process Engineering, Technische Universität Dresden, 01062 Dresden, Germany.

Corresponding author: a.doess@hzdr.de

Abstract

Non-uniform bubble size and liquid velocity distribution in bubble columns lead to gas phase dispersion. This gas phase backmixing is quantitatively modelled in the axial gas dispersion model by the axial gas dispersion coefficient. However, only few gas phase dispersion data are currently available since experimental investigations are expensive and require the application of suitable gas tracers and their reliable detection. In this study a new approach is introduced, which is based on a lock-in measurement of gas fraction modulation. Experiments were carried out in a bubble column of 100 mm diameter operated with air/water and air/glycol-water, respectively. Gas holdup was measured via gamma-ray densitometry in synchronization with the modulated inlet flow. The axial dispersion model was adopted to determine the gas phase dispersion coefficient from phase shift and amplitude damping of the gas holdup frequency response. A sensitivity analysis was performed to derive a proper modulation scheme. The calculated gas phase dispersion coefficients show excellent agreement with data from literature.

Keywords

Bubble column, gas phase dispersion, axial dispersion coefficient, gas flow modulation, frequency response analysis, gamma-ray densitometry.

1. Introduction

Bubble columns are widely applied in the chemical, petrochemical, biochemical and environmental industries, for example for hydrocarbon syntheses, hydrogenation of saturated oils and waste water treatment. These gas-liquid contactors are characterized by a simple construction and low maintenance costs. Mainly, they are preferred for bulk processes with slow reactions and liquid-side mass transfer limitation as well as for processes with strong exothermic behavior (Cheremisinoff et al., 1986, Hertwig et al., 2007, de Haan et al., 2015).

The bubble column's volumetric productivity as well as its mass and heat transfer rates are affected by the prevailing hydrodynamics covering gas holdup, bubble size, dispersion of gas and liquid phase as well as flow regime. Different theoretical approaches exist to link column performance to dispersion and mixing in bubble columns. Overviews about available mixing models are given e. g. by Schlüter et al. (1992), Levenspiel et al. (1998) and Shah et al. (2004). Most important mixing models are e.g. the mixed-cell model (Turner et al., 1990), the tanks-in-series model (Fogler et al., 2005) and the recirculation with cross-flow dispersion (RCFD) model (Degaleesan et al., 1967). The axial dispersion model (ADM) (Nauman et al., 2002, Davis et al., 2003) is the most widely applied one to consider the mixing behavior of the involved phases and was applied for process modelling in absorption columns (Deckwer et al., 1977) and chemical reactors (Stern et al., 1985, Turner et al., 1990 Behin et al., 2013).

Similar to the classical diffusion theory for miscible fluids, dispersion of immiscible fluids, such as gas in bubble columns, is described as a finite superimposing flow in main flow direction (Mangartz et al., 1977). The liquid phase dispersion in bubble columns is caused by rising gas bubbles, which partially carry the liquid upwards - preferentially in the column center - creating a circulating flow pattern with liquid downflow near the column wall (Groen et al., 1996). Gas dispersion in bubble columns, in turn, arises from the variety of bubble rise velocities depending on the evolving bubble size distribution, which is driven by coalescence and breakup events (Rubio et al., 2004). The gas phase dispersion is strongly increased at heterogeneous flow conditions with fast rising large bubbles and swarms of smaller bubbles at comparably low rise velocity (Zahradnik et al., 1996). Dispersion processes are approximated by means of dispersion coefficients D_i for the particular phase i based on residence time measurement data. Since the residence time of the respective phase can hardly be measured directly, appropriate tracer substances (in terms of neutral buoyancy, insolubility, non-reactivity, detectability, Shah et al., 2004) are added and tracked. The residence time of a tracer is considered to be distributed depending on the dispersions magnitude (Mangartz et al., 1977). For example, small dispersion results in a narrow residence time distribution (RTD) of a tracer added as Dirac pulse, while increasing

dispersion widens the RTD (Levenspiel et al., 1998). Here, the dispersion coefficient establishes the functional link between the theoretical mixing model and the measured RTD.

While liquid dispersion in bubble columns has widely been studied (Shah et al., 1978), only few gas phase dispersion data are currently available, which traces back to the fact that their experimental determination is challenging. Usually such experimental investigations are carried out by injecting and capturing a tracer gas of different properties (temperature, elemental composition, radioactivity) than the bulk gas. Depending on the way the (gas) tracer is added, RTD measurements are basically categorized into *steady state* and *non-steady state* methods (Mangartz et al., 1977, Hertwig et al., 2007). Although the dispersion of a (gas) tracer is inherently dynamic, the predominant convection in bubble columns allows the assumption of a stationary tracer concentration profile upon steady state tracer injection (Mangartz et al., 1977). However, such steady state methods require a uniform distribution of the gaseous tracer in the entire column cross-section at the injection height, which is practically not feasible. In contrast, non-steady state methods rely on measuring the tracer concentration downstream the injection point considering its relation to the initial value (Deckwer et al., 1974). Therefore, non-steady state methods preferably apply well-defined tracer injection signals such as jumps, ramps, pulses or periodic functions. While traveling from the injection point towards the downstream measurement positions, the initial tracer signal gets damped in amplitude and shifted in phase by dispersion, which is reflected in the tracer residence time. In the past, several techniques were developed and may be distinguished by the type of tracer and its detection method as well as by the imposed tracer signal (Tab 1). It should be noted that gas dispersion studies in bubble columns operated with pronounced liquid superficial velocity higher than $0.06\,m/s$ (e.g. Kulkarni et al., 1989) are not considered here for brevity and consistency.

In the following we will summarize available reports on previous experimental work in this field. So far, mainly, inert gases were used as tracers in bubble columns. For example, DeMaria et al. (1960), Diboun et al. (1965), Kago et al. (1989), Kawagoe et al. (1989), Shetty et al. (1992) and Kantak et al. (1995) used pure He or He mixed with N_2, Ar or CO_2. The helium concentration was mostly monitored by thermal conductivity analyzers (Diboun et al., 1965, Kago et al., 1989, Kawagoe et al., 1989), mass spectrometry (Shetty et al., 1992, Kantak et al., 1995) or ionization cells (DeMaria et al., 1960). Others used H_2 tracers, which were detected by thermal conductivity analyzers (Carleton et al., 1967, Men'shchikov et al., 1967) or dichloro-difluoromethane (CCl_2F_2) detected by gas chromatography (Wachi et al., 1990) or ionization cell (Towell et al., 1972). Koelbel et al. (1962) replaced the initial gas phase (N_2) by CO and monitored the change at the outlet using infrared gas sensors. A simple approach was used by Joseph et al. (1984). They switched gas supply from nitrogen to pure oxygen and analyzed the gas stream samples with an oxygen sensor. In most

studies the gas was extracted by funnel-shape devices (Diboun et al., 1965, Carleton et al., 1967, Shetty et al., 1992, Kantak et al., 1995) or suction units (Kago et al., 1989, Kawagoe et al., 1989) connected to the respective sensors. Their additional impact on the tracer RTD had to be considered (Wachi et al., 1990, Kawagoe et al., 1989). In few studies short-lived radioisotopes of argon (^{41}Ar) and sodium (^{24}Na) were used as tracers and detected via radiation detectors (Seher et al., 1978, Field et al., 1980). It should also be mentioned that some of the applied techniques required additional sample treating such as gas drying (by heat or other separation principles), sample mixing (Joseph et al., 1984) or additional reference measurement runs (Shetty et al., 1992).

Table 1: Summary of gas dispersion measurement techniques reported in literature.

Tracer substance	Tracer signal	Tracer detection mode	References
CO	sine	infrared gas sensor	Mangartz et al. (1980)
	jump	infrared gas sensor	Koelbel et al. (1962)
CO_2	pulse	mass spectroscopy	Kantak et al. (1995)
	sine	thermal conductivity analyzer infrared gas sensor	Gray et al. (1963), Mangartz et al. (1980)
He, He/N_2, He/Ar, He/CO_2	pulse	thermal conductivity analyzer mass spectroscopy	Diboun et al. (1965), Carleton et al. (1967), Kago et al. (1989), Kawagoe et al. (1989), Shetty et al. (1992), Kantak et al. (1995)
	jump	ionization cell	DeMaria et al. (1960)
CCl_2F_2	pulse	gas chromatography	Wachi et al. (1990)
	jump	electrometer	Towell et al. (1972)
H_2, H_2/N_2	pulse	thermal conductivity analyzer	Carleton et al. (1967), Men'shchikov et al. (1967)
CH_4	sine	infrared gas sensor	Mangartz et al. (1980)
	rectangle	thermal conductivity analyzer	Coulon et al. (1971)
O_2	jump	polarographic oxygen analyzer	Joseph et al. (1984)
^{41}Ar, ^{24}Na	pulse	spectral analysis	Seher et al. (1978), Field et al. (1980)

In the studies listed in Tab 1, tracers were mostly injected according to step or impuls functions (e.g. additive to the normal gas supply or by replacing the original gas phase by the tracer gas). Kramers et al. (1953) and Böxkes et al. (1972) discussed the experimental and mathematical challenges arising with the addition of discontinuous tracer signals to continuous flows and potential errors. Reference measurements from different operating conditions (Joseph et al., 1984, Kago et al., 1989) and mathematical corrections of considerable magnitude were inevitable to obtain feasible results. Furthermore, flow disturbances by sampling or sample guiding internals (Wachi et al., 1990) were often accepted in favor of representativeness of experimental data. Hence, universal applicability of those methods is limited by sampling procedure and guaranteeing of veridic signal transmission behavior.

An alternative approach is the frequency response analysis (FRA) for periodic tracer injections. Periodic tracer injection leads to downstream propagation of a tracer concentration wave. Here, the dispersion causes damping of the tracer concentration wave amplitude and phase shift at a downstream position. A detailed explanation of this method is given by Gray et al. (1961). Mass transfer absorption experiments with square-wave CH_4 and sinusoidal CO_2 tracer inlet were performed by Coulon et al. (1971) and Gray et al. (1963), respectively. They discussed their results with respect to gas phase dispersion based on the amplitude damping and phase shift from inlet and outlet tracer signal. However, the effect of the transient mass transfer behavior was not considered ignoring the influence of the absorption on the shape of the tracer response (Kantak et al., 1995, Vermeer et al., 1981) and possible overestimation of the gas dispersion coefficient (Field et al., 1980, Shetty et al., 1995). Gray et al. (1963) studied the effect of different sinusoidal frequencies and their applicability towards different mixing model approaches. The most comprehensive FRA-based gas dispersion study was performed by Mangartz et al. (1980), where the alteration of the tracer inlet signal was monitored via eight probes mounted at different axial positions. However, although the theoretical approach of FRA was considered very promising, only very few such studies were performed, which can be attributed to the complex measurement system including challenging periodic tracer injection, ensuring negligible interference with the steady state hydrodynamics and linear transmission behavior of the complete system (Gray et al., 1961) as well as difficulties in synchronized downstream detection.

Most of the gas dispersion studies addressed air/water systems only. Increasing the gas phase superficial velocity u_G was found to intensify the gas dispersion, which is even more pronounced at heterogeneous flow conditions due to the formation of larger eddies in the liquid (Mangartz et al., 1977, Shetty et al., 1992). The influence of the liquid superficial velocity, however, was found to be negligible. While the effect of column height on the gas dispersion coefficient can be neglected (Mangartz, et al., 1977, Koelbel et al., 1962), increasing column diameter d was found to significantly boost axial gas dispersion (Mangartz et al., 1977, Kawagoe et al., 1989) and heterogeneity of gas-liquid dispersion (Shetty et al., 1992). Consequently, the gas dispersion coefficient D_G is mostly described by empirical correlations of the form

$$D_G = C_1 \cdot d^{j_1} \cdot C_2 \cdot u_G^{j_2} \cdot C_3 \cdot u_S^{j_3}\,, \tag{1}$$

where

$$u_s = u_G/\bar{\varepsilon} \tag{2}$$

is the bubble swarm velocity, which depends on the mean gas holdup $\bar{\varepsilon}$. Tab 2 summarizes the constants C_i and exponents j_i of Eq. 1 from the literature. Few correlations also considered the contribution of different bubble size classes (Kawagoe et al., 1989), the effects of relative phase velocity u_R (Shah et al., 1978), liquid circulation velocity u_{LC} and bubble slip velocity u_{BS} (Kraume et al., 1989) as well as liquid phase properties (Zehner et al., 1984).

Table 2: Parameters of gas phase dispersion coefficients in bubble columns according to Eq. 1.

Reference	Parameters according to Eq. 1						Column dimensions (*d* - diameter, *H* - height)	Fluid system	Parameter range
	C_1	j_1	C_2	j_2	C_3	j_3			
Men'shchikov et al. (1967)	0	0	1.47	0.72	0	0	$d = 0.30\ m,\ H = 5.00\ m$	air / water	$u_G = 0.008 \dots 0.096\ m/s$
Towell et al. (1972)	19.7	2	1	1	0	0	$d = 0.41\ m,\ H = 2.70\ m$ $d = 1.07\ m,\ H = 5.20\ m$	air/ water	$u_G = 0.008 \dots 0.131\ m/s$ $u_L = 0.007 \dots 0.014\ m/s$
Pilhofer et al. (1978)	0	0	0	0	2.64	3.56	$d = 0.10\ m,\ H =$ n.a	air / water, nitrogen/ n-propanol, air / glycol	$u_G = 0.010 \dots 0.130\ m/s$
Shah et al. (1978)	20	1	$\frac{u_R}{u_G}$	1	0	0	$d = 0.14\ m,\ H = 0.52\ m$	air / water	$u_G = 0.010 \dots 0.050\ m/s$ $u_L = 0.001 \dots 0.010\ m/s$
Field et al. (1980)	56.4	1.33	0	0	1	3.56	$d = 3.20\ m, H = 18.9\ m$	n.a	$u_G = 0.040 \dots 0.055\ m/s$ $u_L = 0.030 \dots 0.045\ m/s$
Mangartz et al. (1980)	50	1.5	0	0	1	3	$d = 0.10\ m,\ H = 1.30\ m$ $d = 0.14\ m,\ H = 2.50\ m$	air / water, nitrogen/ n-propanol, air / glycol	$u_G = 0.010 \dots 0.130\ m/s$ $u_L = 0 \dots 0.060\ m/s$
Joshi et al. (1982) *(data fitting of Koebel et al., 1962, Carleton et al.,1967, Men'shichikov et al.,1967, Towell et al.,1972, Seher et al.,1979, Mangartz et al.,1980)*	110	2	$\frac{1}{\varepsilon}$	2	0	0	$d = 0.09 \dots 1.07m$ $H = 0.60 \dots 5.10\ m$		$u_G = 0.001 \dots 0.130\ m/s$ $u_L = 0 \dots 0.060\ m/s$
Heijnen et al. (1984) *(data fitting of Carleton et al.,1967, Towell et al.,1972, Field et al.1980, Mangartz et al., 1980)*	78	1.5	1	1.5	0	0			$u_G = 0.008 \dots 0.130\ m/s$ $u_L = 0 \dots 0.060\ m/s$
Zehner et al. (1984) (*data fitting of Koebel et al., 1962, Towell et al.,1972, Mangartz et al.,1980*)	$\frac{\zeta \cdot g \cdot \Delta\rho}{2 \cdot \rho_L}$	2	1	2	1	-3	$d = 0.08 \dots 3.20m$ $H = 1.30 \dots 18.9\ m$		
Kraume et al. (1989) (*data fitting of Koebel et al., 1962, Towell et al.,1972, Mangartz et al.,1980*)	$0.5 \left(\frac{u_{LC}}{u_{BS}}\right)^3$	1	0	0	1	1			
Wachi et al. (1990)	20	1.5	1	1	0	0	$d = 0.20\ m,\ H = 4.50\ m$ $d = 0.50\ m,\ H = 4.50\ m$	air / water, CMC, ethanol	$u_G = 0.029 \dots .0.456\ m/s$
Kantak et al. (1995)	0.2	1.25	0	0	1	1	$d = 0.15\ m,\ H = 2.70\ m$ $d = 0.25\ m,\ H = 2.70\ m$	air /water	$u_G = 0.010 \dots 0.18\ m/s$ $u_L = 0.005 \dots 0.03\ m/s$
Kawagoe et al. (1989)	$D_G = 0.66\, D_{G,1} + 0.39 D_{G,2} + 0{,}0078\ (u_S \cdot H\ )$ $D_{G,1} = 26.2 \cdot {u_s}^{3.03} \cdot d^{1.79}$ $D_{G,2} = 19.4 \cdot {u_s}^{3.4} \cdot d^{2.1}$						$d = 0.16\ m,\ H = 2.00\ m$ $d = 0.29\ m,\ H = 2.00\ m$	air / water, sodium sulfate, CMC	$u_G = 0.009 \dots 0.03\ m/s$ $u_S = 0.270 \dots 0.54\ m/s$

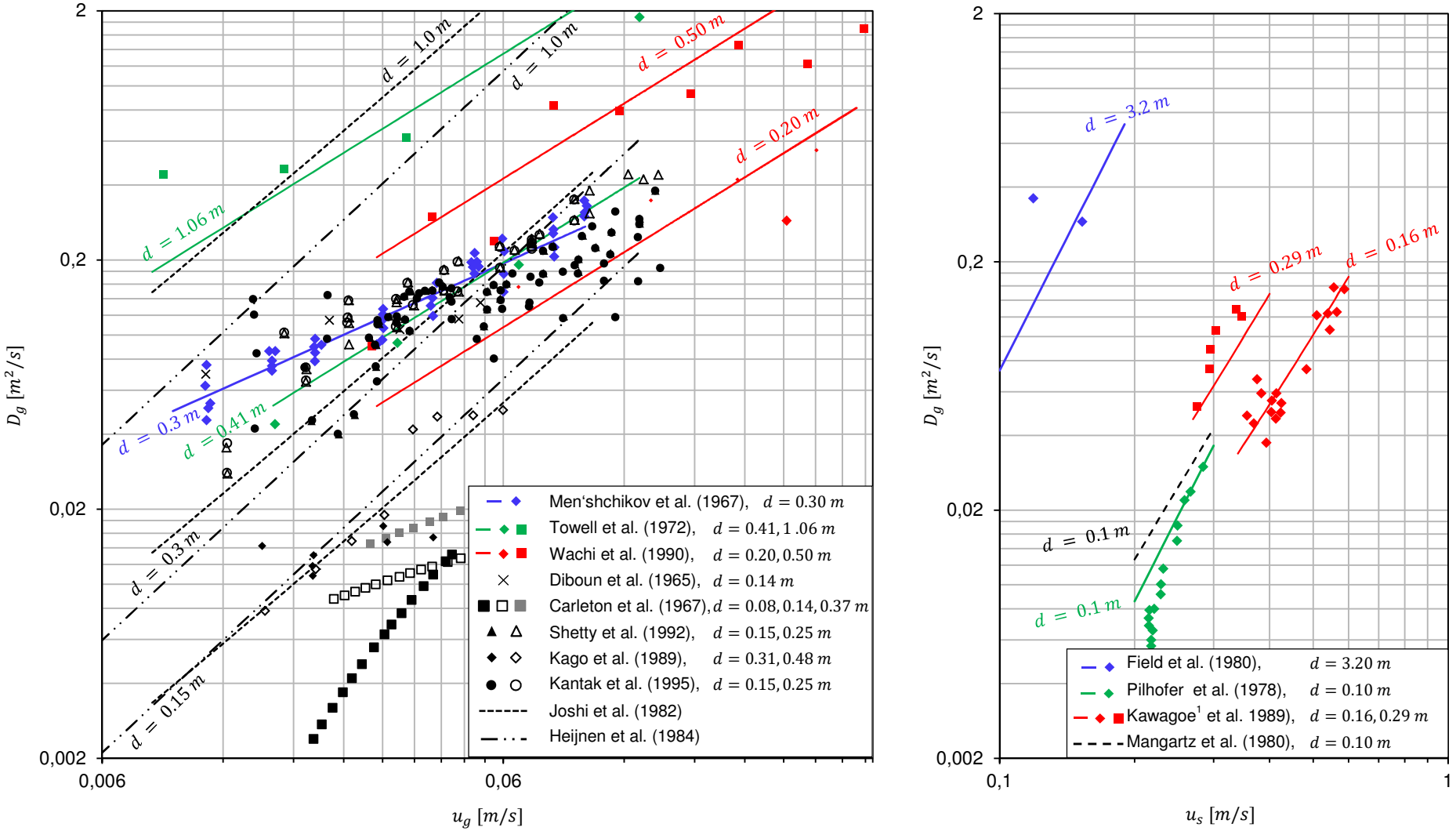

Figure 1: Experimental data and empirical correlations for gas phase dispersion coefficients in bubble columns functionalizing (left) superficial gas velocity and (right) bubble swarm velocity (data shown for air/water systems only).

1) D_G calculated according to experimental data of $D_{G,1}$ and $D_{G,2}$, see Tab. 2

Fig. 1 summarizes available experimental data and derived empirical correlations for the gas phase dispersion coefficient in bubble columns, accounting for the effects of (left) superficial gas velocity and (right) bubble swarm velocity, respectively. It should be noted that only experimental data for air/water systems, which is the vast majority of the available data, are shown for a clear and concise overview as well as for easier comparability. Experimental data and corresponding correlations are accordingly color-coded. Black lines indicate correlations (Joshi et al., 1982, Heijnen et al., 1984) fitted against data from several studies (Tab. 2). There is a fair agreement in the general effect of the superficial gas velocity u_G shown by the similar slopes of lines and experimental data of respective studies. Although, the dispersion coefficients were found to increase with increasing column diameter (compare Wachi et al., 1990, Carleton at al., 1967, and Kago et al., 1989), the dispersion coefficients obtained from different authors for the same column diameter differ significantly (compare Diboun et al., 1965, Carleton et al., 1967, Shetty et al., 1992 and Kantak et al., 1995 for $d \approx 0.15\,m$). Similar scattering was also found for other column diameters such as $d \approx 0.30\,m$ and $d \approx 0.50\,m$. Plotting the dispersion coefficients against the bubble swarm velocity u_s was proposed to reduce the data scattering as shown in the right plot of Fig. 1. Although not shown here, Mangartz et al. (1980) confirmed that the gas holdup ε accounts fairly for the effects of liquid properties and sparging devices on the dispersion. However, the available database is still rather small.

It can be concluded that the prediction of the gas phase mixing behavior in bubble columns is still subject to pronounced uncertainties, in particular at low bubble swarm velocities. Although not fully recorded, it is hypothesized that results of previous studies were remarkably influenced by the applied measurement approach indicated by the systematic deviations (offsets) as discussed above.

Thus, a new approach, recently patented by Hampel (2015), will be introduced in this paper. Contrary to the above mentioned methods using tracer substance addition this approach is fully non-invasive. Here the gas inlet flow is slightly modulated in its flow rate and thus produces a gas holdup disturbance wave moving upward with the gas phase. The modulated gas holdup recorded via gamma-ray densitometry in a synchronized manner and with a special count-wise data collecting mode to ensure lock-in detection with a highest signal-to-noise ratio. In the following we will introduce the method in detail, discuss experimental findings and present results of a confidence level and sensitivity analysis.

2. Materials and methods

2.1 Theoretical model

The new approach bases on the axial dispersion model (ADM) (Hertwig et al., 2007, Deckwer et al., 1985, Gray et al. 1961, Shah et al., 1978, Degaleesan et al., 1967). Being applied to the dispersed gas phase, this model (Eq. 3) assumes, that the gas in the column rises with a mean rise velocity u_S and is being dispersed in axial direction x, which is quantified by the axial dispersion coefficient D_G. Hence, gas phase holdup follows the linear partial differential equation

$$\frac{\partial \varepsilon}{\partial t} = D_G \frac{\partial^2 \varepsilon}{\partial x^2} - u_S \frac{\partial \varepsilon}{\partial x}. \tag{3}$$

Now we assume a column with modulation in gas flow rate, represented by the modulated superficial gas velocity

$$u_G(t) = \bar{u}_G\big(1 + A\, cos(\omega\, t)\big) \tag{4}$$

Here $\bar{u}_G$ is the average value and A the modulation amplitude of the superficial gas velocity, which should be of low magnitude (see section 2.4). $\omega = 2\pi f_{mod}$ is the angular modulation frequency. Then the boundary condition at $x = 0$ is

$$\varepsilon_{x=0}(t) = \bar{\varepsilon}\left(1 + A\, cos(\omega t)\right) = \bar{\varepsilon} + \frac{1}{2}\bar{\varepsilon}A\big(e^{i\omega t} + e^{-i\omega t}\big). \tag{5}$$

Further we are only interested in the modulated part and therefore refer to $A_\varepsilon = \bar{\varepsilon}A$ as the amplitude of the obtained gas holdup signal. The following mathematical treatment considers only one of the harmonic terms from Eq. 5. Following the method of separation of variables the ansatz

$$\varepsilon(x,t) = \varepsilon(t)\, \varepsilon(x) = e^{j\omega t}\, \varepsilon(x) \tag{6}$$

is made. Insertion into Eq. (3) gives

$$\left[\frac{\partial^2 \varepsilon}{\partial x^2} - \frac{u_S}{D_G}\frac{\partial \varepsilon}{\partial x} - \frac{j\omega}{D_G}\varepsilon\right] e^{j\omega t} = 0. \tag{7}$$

Under the assumption that $\lim_{x\to\infty}|\varepsilon(x,t)| = 0$, the physically plausible solution of Eq. 7 is

$$\varepsilon(x,t) = e^{i\omega t} e^{\frac{u_S}{2D_G}\left[1-\sqrt{1+4i\omega D_G/{u_S}^2}\right]x} \quad . \tag{8}$$

Eventually, Eq. 8 can be rearranged into real and imaginary part:

$$\varepsilon(x,t) = e^{i\omega t} \cdot e^{\frac{u_S}{2D_G}\left[1-\frac{1}{\sqrt{2}}\left(\sqrt{1+\sqrt{1+\frac{16\omega^2{D_G}^2}{u_S^4}}}\right)\right]x} \cdot e^{i\frac{u_s}{D_G\sqrt{8}}\left[-\sqrt{\sqrt{1+\frac{16\omega^2{D_G}^2}{u_S^4}}-1}\right]x} \tag{9}$$

The solution describes a harmonic signal ($e^{i\omega t}$) whose amplitude is damped and whose phase is shifted. Applying complex number calculus the expression can be split to yield the amplitude damping V and the phase shift $\Delta\phi$.

$$V = |\varepsilon(x,t)| = \exp\left[\frac{u_S x}{2D_G}\left(1-\frac{1}{\sqrt{2}}\left(\sqrt{1+\sqrt{1+\frac{16\omega^2{D_G}^2}{u_S^4}}}\right)\right)\right] \tag{10}$$

and

$$\Delta\phi = \arg\{\varepsilon(x,t)\} = \frac{u_S x}{2D_G}\left(-\frac{1}{\sqrt{2}}\left(\sqrt{\sqrt{1+\frac{16\omega^2{D_G}^2}{u_S^4}}-1}\right)\right) \tag{11}$$

Eq. 10 and 11 describe amplitude damping and phase shift relative to the harmonic function at $x = 0$. Note that in following formulations $V = A_\varepsilon(x_2)/A_\varepsilon(x_1)$ and $\Delta\phi = \phi_1(x_2) - \phi_2(x_1)$ describe relative amplitude damping and phase shift between two axial positions x_1, x_2 (see Fig. 2). This implies prior amplitude damping and phase shift between x_0 and x_1, which must be taken into account (see section 2.3 and 2.4) in all calculations.

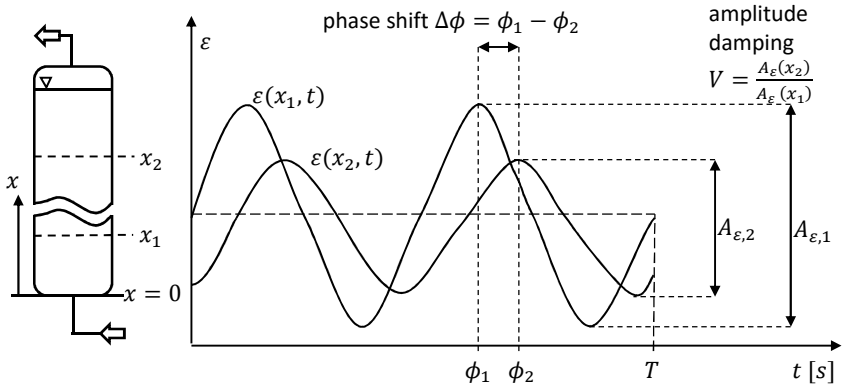

Figure 2: Gas holdup modulation and its parameters in two axial positions.

Looking for a simple analytical solution, Mangartz et al. (1977) and Gray et al. (1961) substituted the complex square root term in Eq. (8), using the Taylor series expansion of the binominal series $\sqrt{1+y}$

$$\sqrt{1+y} = \sum_{k=0}^{k} \binom{1/2}{k} y^k \quad \text{with} \quad y = \left(i \cdot 4\frac{\omega D_g}{{u_S}^2}\right) \quad \text{valid for} \quad |y| < 1. \tag{12}$$

Thus, Eq. 8 can be approximated considering multiples of $k = 2$. While even terms contribute to the solution of the amplitude ratio, uneven terms contribute to the imaginary part and therefore to the phase shift. The validity criteria of Eq. 12 can be expressed in terms of the critical frequency $f_c = {u_S}^2/8\pi D_g$ defining the maximum possible frequency for the application of the Taylor series expansion. The resulting expressions, which depend on the largest considered value of k, are summarized in Tab. 3.

Table 3: Solutions of Eq. 11 truncated after different values of k.

k	*Solution for V*		*Solution for $\Delta\phi$*	
$k \to \infty$ (exact solution)	Eq. 10		Eq. 11	
$k = 2$	$\exp\left[-\frac{\omega^2 D_G}{u_S^3} x\right]$	(13)	$-\frac{\omega}{u_S} x$	(14)
$k = 4$	$\exp\left[-\frac{\omega^2 D_G}{u_S^3} x \cdot \left(1 - 5\frac{\omega^2 {D_G}^2}{u_S^4}\right)\right]$	(15)	$-\frac{\omega}{u_s} x \cdot \left(1 - 2\frac{\omega^2 {D_G}^2}{u_S^4}\right)$	(16)

Mangartz et al. (1977) and Gray et al. (1961) ignored all terms of $k > 2$, which were claimed to be much smaller than 1. To verify this approach, amplitude damping V and phase shift $\Delta\phi$ resulting from the truncated Taylor series expansion (TS) were compared with the exact solution (ES) given by the exact solution of the ADM and expressed in terms of relative errors $RE_V = |(V_{TS} - V_{ES})/V_{ES}|$ and $RE_\phi = |(\Delta\phi_{TS} - \Delta\phi_{ES})/\Delta\phi_{ES}|$, respectively. The relative

errors RE were exemplarily calculated for two different dispersion coefficients D_G of typical magnitude and their corresponding bubble swarm velocities u_s extracted from Fig. 1 (right)

$$P_1 = \begin{pmatrix} D_{G,1} \\ u_{S,1} \end{pmatrix} = \begin{pmatrix} 0.02\ m^2/s \\ 0.25\ m/s \end{pmatrix}$$
$$P_2 = \begin{pmatrix} D_{G,2} \\ u_{S,2} \end{pmatrix} = \begin{pmatrix} 0.11 m^2/s \\ 0.38\ m/s \end{pmatrix}.$$

The relative errors of the Taylor series expansions for $k = 2$ and $k = 4$ and an assumed longitudinal distance $x = 1\,m$ are plotted in Fig. 3 (left) against the normalized frequency $\bar{f} = f/f_c$, where f_c is $0.1243\ Hz$ and $0.0455\ Hz$ for P_1 and P_2, respectively.

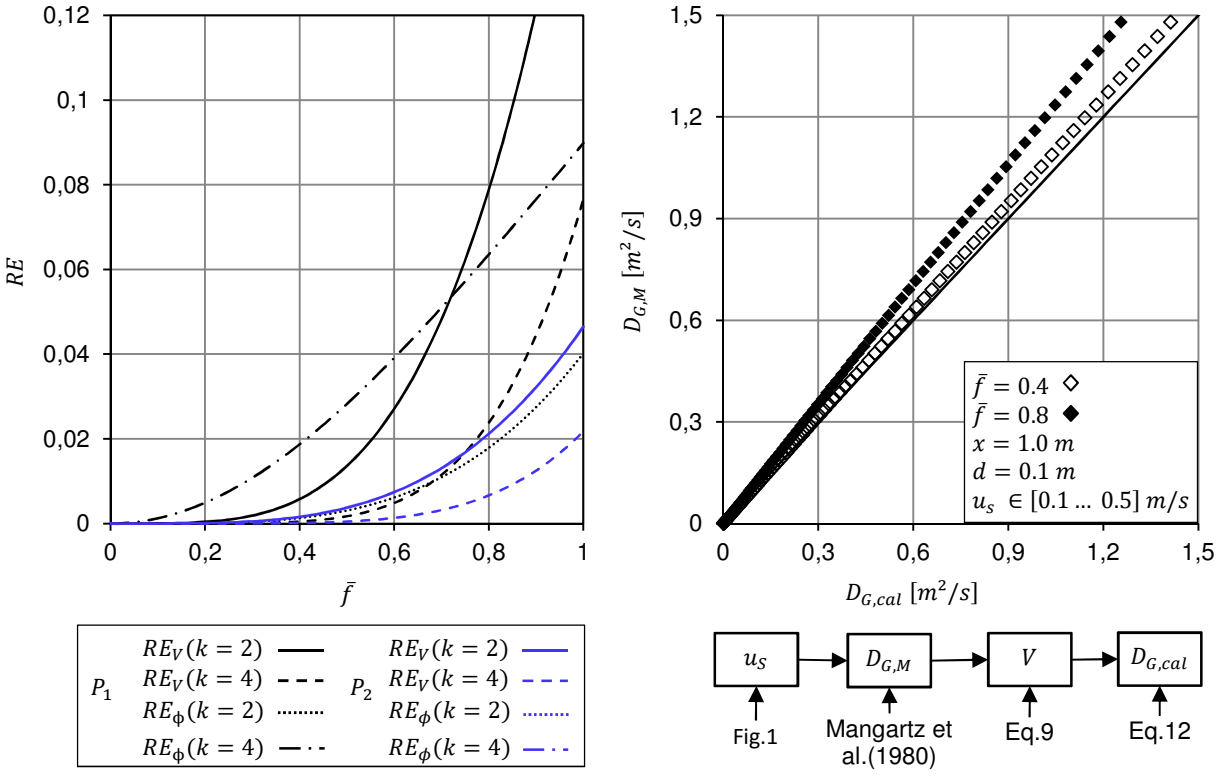

Figure 3: Relative error for the truncation of the Taylor series expansion (left) and deviation of the dispersion coefficient calculated from Eq. 12 at $\bar{f} \epsilon [0.4; 0.8]$ for selected operating conditions, i.e. P_1 and P_2.

The graphs of RE_ϕ for P_1 coincide with the respective ones of P_2, indicating that (in contrast to RE_V) the relative error RE_ϕ depends rather on modulation frequency than on the dispersion values. The early truncation of the Taylor series expansion invokes severe deviations near the critical frequency f_c ($\bar{f} \to 1$). The right sub-plot in Fig. 3 shows the resulting deviation of D_G between ADM and Eq. 13 for two frequencies $\bar{f} \in [0.4; 0.8]$. The calculation procedure is schematically drawn below the figure. For varying u_s (taken from Fig.

1), prediction values $D_{G,M}$ were calculated using the correlation of Mangartz et al. (1980). From the values $D_{G,M}$ the corresponding exact amplitude damping V_M was calculated by the complex notation of the ADM (Eq. 8). The deviation between $D_{G,M}$ and the dispersion coefficient calculated from the truncated solution in Eq. (13), $D_{G,cal}$, is shown in the parity plot. In particular for higher dispersion, D_G is underestimated by the truncated expression. Thus, the approximation of the truncated Taylor series expansion is only recommended for frequencies $f/f_c < 0.5$ and low dispersion. Since the former requires rather small frequencies, which is technically challenging, the new method was developed based on the exact solutions by transforming Eq. 10 and Eq. 11, respectively, and substituting $K_1 = u_S \cdot x/2$ and $K_2 = 16\omega^2/u_S^4$, giving

$$D_G = \sqrt{\frac{K_1^4}{4\Delta\phi^4}\left(K_2 - \frac{4\Delta\phi^2}{K_1^2}\right)} \tag{17}$$

and

$$D_G = \frac{4}{K_1 K_2}\left(\frac{\ln(V)^4\, D_G^3}{K_1^3} - 4\frac{\ln(V)^3\, D_G^2}{K_1^2} + 5\frac{\ln(V)^2\, D_G}{K_1} - 2\ln(V)\right). \tag{18}$$

Eq. 18 is iteratively solved using the initial value $D_G^0 = 10^{-4}\, m^2/s$. Both equations for the gas phase dispersion coefficient D_G depend on the parameters V and $\Delta\phi$, respectively, as well as on the process parameter u_S and the adjustable measurement parameters x, ω of the new FRA method. Thus, a sensitivity analysis was performed to determine the model accuracy and to predict proper measurement parameters.

2.2 Sensitivity analysis

A comprehensive analysis of the sensitivity requires consideration of all involved parameters $(V, \Delta\phi, x, f_{mod})$ in multiple steps. For ease of illustration, a simplified approach is presented, which is based on the sensitivity analysis for the variation of x and f considering a previously defined parameter range of u_S and D_G , i.e. P_1 and P_2 deduced from Fig. 1. The theoretical values of V and $\Delta\phi$ for the chosen boundaries of the parameter range were calculated applying Eq. 10 and Eq. 11, respectively. By calculating the difference $\Delta V = |V(P_2) - V(P_1)|$ and $\Delta\phi^* = |\Delta\phi(P_2) - \Delta\phi(P_1)|$ at each point of the (x, f) map the sensitivity can be estimated and accordingly, proper measurement parameters can be selected.

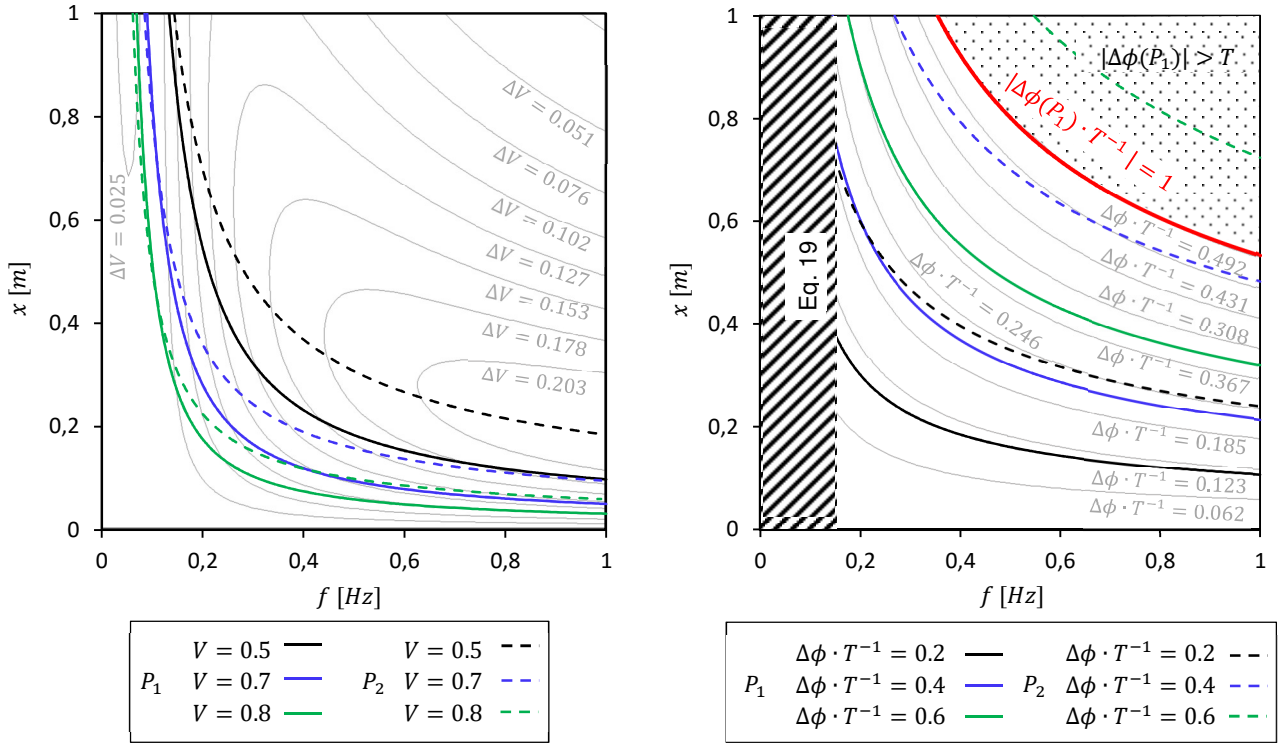

Figure 4: Sensitivity of amplitude damping ΔV and normalized phase shift $\Delta\phi^* \cdot T^{-1}$ with respect to measurement distance x and modulation frequency f for selected operating conditions, i.e. P_1 and P_2.

Fig. 4 shows the magnitude of ΔV and $\Delta\phi^*$ encoded by light grey isolines, which indicate the model sensitivity. For easier visualization and understanding the period time T was used for normalization of phase shift difference. In Fig. 4 high values of ΔV and $\Delta\phi^*$ imply better accuracy of the results, since the variation of the parameters due to dispersion shows a high sensitivity for the specific process parameters. In other words, already small changes in D_G for a constant u_s noticeably change V and $\Delta\phi$ respectively. These plots allow conclusions on proper modulation and measurement parameters, which is, however, a compromise between high sensitivity and practical amplitude damping or phase shift in terms of technical feasibility. For example, high sensitivity for the amplitude damping is obtained at values of about $V \approx 0.5$. Since V is a relative value (see section 2.1), the absolute signal magnitude suffers from previous amplitude damping below the respective axial coordinate. Therefore the evaluation of sensitivity always requires consideration of the axial position of the measurements.

The iso-lines for the amplitude damping highlight furthermore that high frequencies with small axial displacements or vice versa are preferred. Obviously hydrodynamics govern the upper limits of modulation frequency (see section 2.3), which is not accounted for in this sensitivity analysis.

The sensitivity of the phase shift $\Delta\phi$ is mainly determined by the axial displacement. The validity area of the (x, f) map with regard to $\Delta\phi$ is restricted by the root expression in Eq. 17 to avoid complex results, which is represented by the condition

$$|\Delta\phi| > \phi_c, \quad \text{with } \phi_c = \frac{\omega x}{u_S}. \tag{19}$$

Violation of this condition for the selected parameters can be expected for modulation frequencies $f_{mod} < 0.14Hz$, whereat the axial position showed only marginal influence on Eq.(19). Secondly, discretization of the total phase shift for values $|\Delta\phi| > T$, was not possible for the employed data acquisition system, which becomes crucial for low dispersion (P_1). This restriction is shown by the red line of $|\Delta\phi(P_1) \cdot T^{-1}| = 1$ in Fig. 4 and thereby gives the upper limits of x and f, respectively. While the restriction $|\Delta\phi| > \phi_c$ is mainly determined by the measurement system, $|\Delta\phi| > T$ to a certain extent is specific for the present dispersion. As the graph for $\Delta\phi \cdot T^{-1} = 0.6$ shows, measurements at high x and f are possible for higher dispersion values of P_2, although the same conditions for the lower dispersion of P_1 could result in false interpretation of phase shift. The information of the above described method was used for the estimation of maximum achievable measurement accuracy in terms of total signal magnitude and interpretability. Considering the technical limitations of the measurement system, which is presented in section 2.4, the analysis of V was determined to be more promising for dispersion measurement and for the calculation of D_G.

2.3 Modulation influence on gas phase dispersion

The influence of the gas holdup modulation on the gas phase dispersion was analyzed to confirm that the column's mixing characteristics as well as linearity of transmission behavior is only marginally influenced by the selected holdup modulation intensity. Following the recommendation from Deckwer et al. (1985) for modelling of gas holdup in bubble columns, the correlation of Bach et al. (1977) given as

$$\frac{\varepsilon_B}{1-\varepsilon_B} = 0.115 \left[u_G \frac{g\Delta\rho\rho_l}{\mu_l}\right]^{0.23} \tag{20}$$

was used for calculation of u_g-values of an assumed symmetric modulation $\varepsilon(t)$ (see Eq. 5). Resulting values of $u_S(\varepsilon(t))$ were used in Mangartz' equation (Mangartz et al., 1980, see Tab. 2) to calculate $D_{G,M}(\varepsilon(t))$. Fig. 5 shows the effect of the modulation holdup amplitude A_ε on the gas phase dispersion coefficient, shown in terms of upper and lower dispersion values of P_1 and P_2 (reflecting minimum and maximum values of $\varepsilon(t)$) respectively.

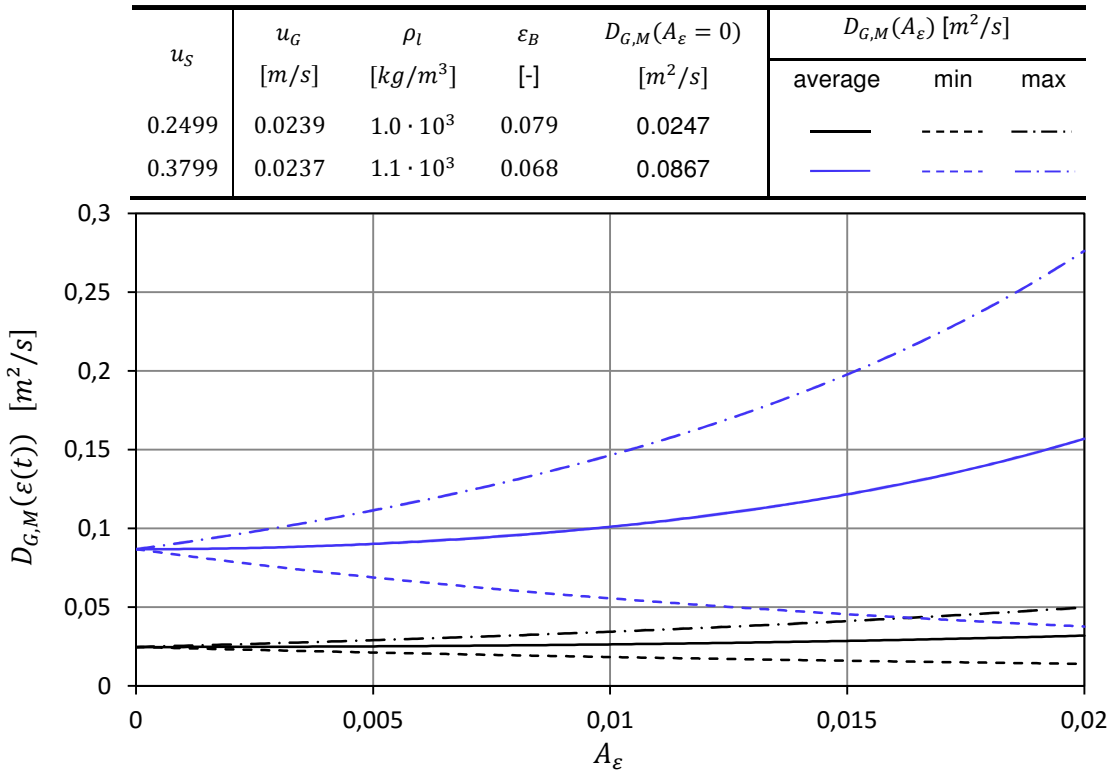

Figure 5: Effect of modulation amplitude A_ε on estimated dispersion coefficients, shown for $P1$ and $P2$.

Both cases show an asymmetric behavior, originated in the exponential nature of Mangartz' equation concerning u_s. Fig. 5 shows that already small holdup modulation in the range of $A_\varepsilon = 0.01 \ldots 0.015$ results in notable changes of dispersion coefficient. However, since the column virtually operates between the extreme cases, the *'average'* mixing behavior is expected to coincide fairly with the stationary counterpart as long as modulation $A_\varepsilon \leq 0.01$.

2.4 Experimental setup

The feasibility of the proposed periodic gas flow rate modulation technique for the determination of the gas dispersion coefficient was demonstrated in a bubble column of $0.1m$ inner diameter operated at $p = 1\,bar$ and $\vartheta = 22\,°C$. Tap water ($\rho = 1000\,kg/m^3$ and $\eta = 2 \cdot 10^{-3}\,Pa\,s$) and glycol ($\rho = 1100\,kg/m^3$ and $\eta = 40 \cdot 10^{-3}\,Pa\,s$) were used as liquid phases and the unaerated liquid height was $1.5\,m$ and $0.8\,m$, respectively. Air was used as the gas phase and introduced at the bottom of the column from a sparger containing 42 needles with $0.2\,mm$ inner diameter equally distributed in the cross-section (Azizi et al., 2016). Experiments were performed at a gas phase superficial velocity $u_G = 0.039\,m/s$, which corresponds to bubble swarm velocities of approximately $u_S = 0.23\,m/s$ and $u_s = 0.38\,m/s$ for water/air and glycol/air, respectively. The required modulation amplitude in gas

holdup of $A_\varepsilon = 0.01$ was represented by a variation in superficial gas velocity of $u_g = 0.005\, m/s$.

The periodic gas flow modulation was adjusted applying a sinusoidal voltage signal to the $10\, V$ input of the flow meter (OMEGA, FMA-2611-10VOUT), whereat mean value, sinusoidal magnitude and modulation frequency were individually adjusted. The amplitude damping and phase shift of the gas holdup was obtained from gamma-ray densitometry measurements. Gamma-ray densitometry is based on the attenuation of a photon flux released from the gamma-ray source while penetrating materials of certain thickness, density and atomic number. The resulting photon flux can be detected via appropriate detectors. Therefore, the bubble column was installed between the isotopic source and the radiation detector arc of a high-resolution gamma-ray tomography system (Hampel et al., 2007, Bieberle et al., 2007). The in-house developed measurement system was already successfully applied to quantify and visualize phase fractions in various multiphase flow applications, for example in chemical reactors (Leon et al., 2013, Tschentscher et al., 2013, Bieberle et al., 2013, Härting et al., 2015, Rollbusch et al., 2015) and technical devices such as pumps (Neumann et al., 2016) or viscous couples (Bieberle et al., 2015).

Radiation of an isotopic source ^{137}Cs with an activity of 185 GBq and a photon energy of 662 keV was used and collimated to a fan beam of $2\, mm$ height towards the detector arc (Fig. 6). The radiation detector arc has a 44° acquisition angle with 320 single detectors, thereof 80 in the radiation shade of the column (illustrated as darker area in Fig. 6). The detector elements, each of $2\, mm \times 8\, mm$ size, consist of a scintillation crystal, an avalanche photo diode and a charge sensitive preamplifier and are operated in pulse mode to count the impacting photons during a certain period of time. The applied energy discrimination allows very accurate measurements by counting only the non-scattered gamma ray photons (Bieberle et al., 2007).

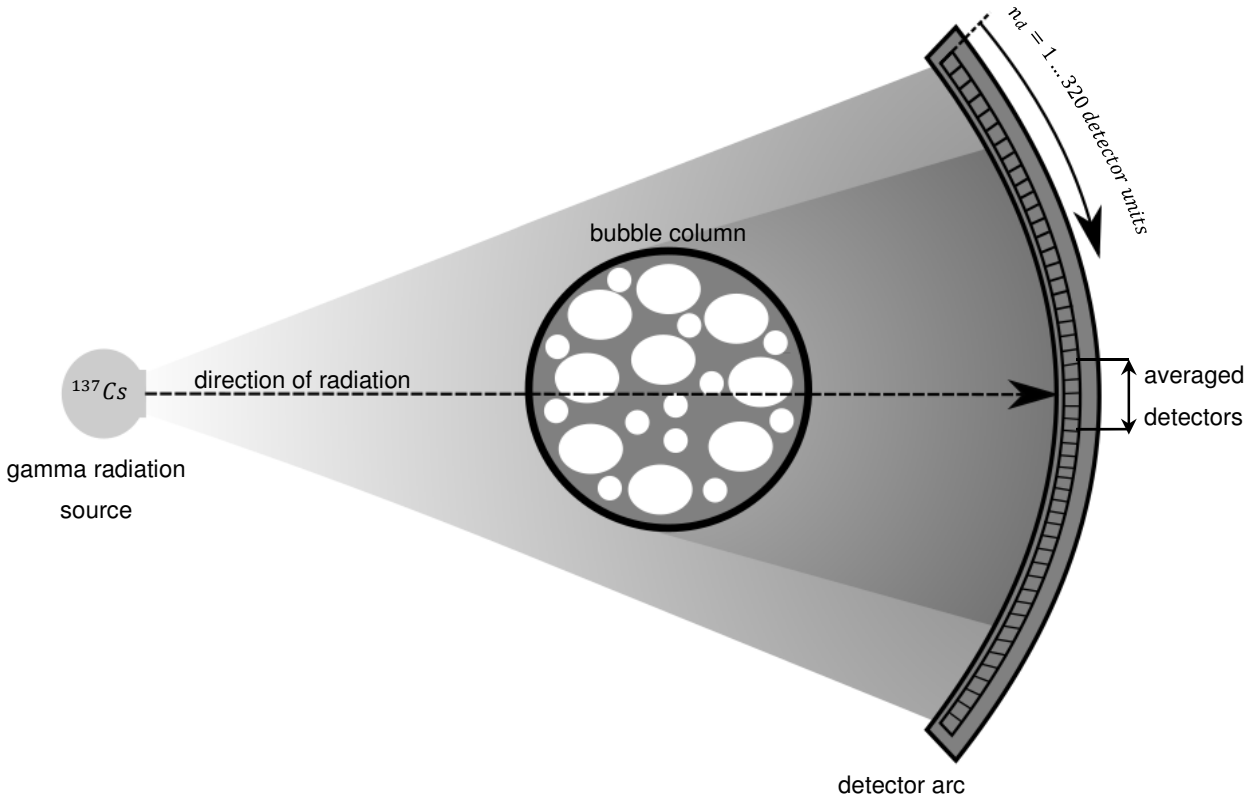

Figure 6: Set-up of gamma-ray densitometry measurement system (column not to scale)

To obtain gas holdup data, measurements at two-phase flow conditions are being made and scaled to reference scans on a gas-free filled column. With the gamma ray densitometer we obtain count rates for empty column ($\dot{N}_G$), unaerated liquid-filled column ($\dot{N}_L$) and aerated column ($\dot{N}_{GL}$). Moreover there is always a non-zero dark count rate $\dot{N}_d$, that is counting of stray radiation events. From these count rates we can compute so called extinction values from the exponential attenuation law for radiation, giving

$$E_{GL} = \log\left(\frac{\dot{N}_G - \dot{N}_d}{\dot{N}_{GL} - \dot{N}_d}\right), \tag{20}$$

$$E_L = \log\left(\frac{\dot{N}_G - \dot{N}_d}{\dot{N}_L - \dot{N}_d}\right). \tag{21}$$

E_L denotes radiation extinction in the unaerated column and E_{GL} for the aerated column. Eventually we get the gas holdup as

$$\varepsilon = 1 - \left(\frac{E_{GL}}{E_L}\right), \tag{22}$$

Typically the low photon flux from gamma ray sources requires longer acquisition intervals for accurate gas fraction measurement. They are typically much longer than the modulation period. Hence we applied a lock-in detection scheme for the gas flow modulation method. There the detector data acquisition is synchronized with the signal generator for the flow meter, which provides a trigger signal at the beginning of each modulation period during the whole measurement time. The radiation detection events are then ensemble-averaged by summing them within n_s equidistant time intervals in each modulation period. Practically, the minimum possible length of such an interval is $45\,ms$, which is dictated by the limited data transfer rate of the used electronics. Thus, to obtain a constant value of $n_s = 50$ samples for each period, the upper limit for the modulation frequency is $f_{max} = 0.44\,Hz$, which corresponds to a period time $T = 2.25\,s$.

The temporal distribution of photon count detection events $N = \dot{N}_\iota \cdot t_s$ is statistically described by a Poisson distribution with $\lambda = N$, expected value $E[\lambda] = N$ and variance $Var[\lambda] = N$. Note that each t_s is the cumulated time of all averaged detection events for a single n_s. Expected values for the reference case count rates (Eq. 21) with applied dark count rate correction were $\dot{N}_G = 9500\,s^{-1}$ and $\dot{N}_L = 4000\,s^{-1}$. Comparison of statistical distribution of quantities with high difference in expected values can be achieved by normalizing the standard deviation $s[\lambda] = \sqrt{Var}$ with the expected value $E[\lambda]$ according to

$$\frac{s[N]}{E[N]} = \frac{\sqrt{Var[N]}}{N} = \frac{1}{\sqrt{N}} = \frac{1}{\sqrt{\dot{N}_i \cdot t_s}} = \sigma_i. \tag{23}$$

By increasing t_s, the coefficient of variance σ_i can be decreased resulting in higher statistical accuracy can be achieved. To correlate σ_i with the relative statistical error in calculated gas holdup values $\Delta\varepsilon$, Eq. 22 together with Eq. 20 and 21 are combined, giving

$$\varepsilon = 1 - \left(\frac{\ln\left(\frac{\dot{N}_G}{\dot{N}_{GL}}\right)}{\ln\left(\frac{\dot{N}_G}{\dot{N}_L}\right)} \right). \tag{24}$$

The relative error $\Delta\varepsilon$ of Eq. 24 is obtained by multiplying σ_i to the corresponding partial derivates

$$\Delta\varepsilon = \pm\frac{\partial\varepsilon}{\partial\dot{N}_G}\sigma_G \pm \frac{\partial\varepsilon}{\partial\dot{N}_{GL}}\sigma_{GL} \pm \frac{\partial\varepsilon}{\partial\dot{N}_L}\sigma_L. \tag{25}$$

We assume a modulation amplitude of $A_\varepsilon = 0.01$ (see section 2.3) and $\bar{\varepsilon} = 0.20$ at axial position x. Corresponding count rate of aerated liquid column would be $\dot{N}_{GL} = 4755\,s^{-1}$ with

periodic part of $\dot{N}_{mod} = 82\ s^{-1}$, representing the damped amplitude A_ε at x. Since $\dot{N}_{mod} \ll \dot{N}_L$ and therefore $\sigma(\dot{N}_{mod}) > \sigma_L$, the minimum required t_s is determined by the dynamic modulated part. Thus, for calculation of t_s, the assumptions $\sigma_G, \sigma_L \to 0$ and $\sigma_{GL} = \sigma(\dot{N}_{mod})$ can be made, if only the dynamic part is investigated. Eqn. 25 then simplifies to

$$\Delta\varepsilon = \frac{\partial\varepsilon}{\partial\dot{N}_{GL}}\sigma_{GL} = \left(\dot{N}_{mod} \cdot \ln\left(\frac{\dot{N}_G}{\dot{N}_L}\right)\right)^{-1} \cdot \sigma_{mod} = \left(\dot{N}_{mod} \cdot \ln\left(\frac{\dot{N}_G}{\dot{N}_L}\right) \cdot \sqrt{\dot{N}_{mod} \cdot t_s}\right)^{-1} = \Delta A_\varepsilon\ . \tag{26}$$

Since ΔA_ε represents an variation in holdup amplitude, the variance in phase shift is not influenced by t_s, but by the temporal resolution of the electronics instead. Measured amplitudes of the holdup periods depend on t_s.

The relative amplitude damping V (between x_0 and x_1) is given as

$$V = \frac{A_\varepsilon(x_1)}{A_\varepsilon(x_0)} = \frac{0.01}{A(x_0)}. \tag{27}$$

Similar to Eq. 25, partial derivates of Eq. 27 give a correlation for ΔV as

$$\Delta V = \frac{\partial V}{\partial A_\varepsilon(x_1)}\Delta A_\varepsilon(x_1) \pm \frac{\partial V}{\partial A_\varepsilon(x_0)}\Delta A_\varepsilon(x_0) = \frac{\Delta A_\varepsilon}{A_\varepsilon(x_0)} \pm \left(-\frac{A_\varepsilon \cdot \Delta A_\varepsilon(x_0)}{A_\varepsilon(x_0)^2}\right). \tag{28}$$

Since the amplitude in holdup (and therefore $\dot{N}_{mod}$) decreases with increasing height position in the column, the highest measurement position x_1 represents the maximum of ΔA_ε while $\Delta A_\varepsilon(x_0) = \Delta A_\varepsilon(x_1)$ was used as approximation to describe the maximum relative variation in amplitude damping by

$$\Delta V_{max} = \Delta A_\varepsilon\left(\frac{1}{A_\varepsilon(x_0)} - \frac{V}{A_\varepsilon(x_0)}\right)\frac{1}{V} = \Delta A_\varepsilon\left(\frac{V}{A_\varepsilon} - \frac{V^2}{A_\varepsilon}\right)\frac{1}{V} = \frac{\Delta A_\varepsilon}{A_\varepsilon}(1 - V). \tag{29}$$

Investigation of Eq. 10 for a given, symmetric relative error RE_{D_G} showed a non-symmetric response RE_V with varying magnitude during one period. Therefore for a given relative variation RE_{D_G}, corresponding variation in RE_V was calculated by assuming the maximum of $RE_V(RE_{D_G})$ as constant for the whole period. Eventually, each $RE_V(RE_{D_G})$ was assigned to a value of ΔV_{max} (Eq. 29), allowing estimation of the relative error RE_{D_G} for varying t_s. Fig.7 shows examples for dispersion P_1, P_2.

f_{mod} [Hz]	x [m]	dis-persion	V [/]	legend
0.3	0.3	P_1	0.524	
		P_2	0.644	
	0.8	P_1	0.179	
		P_2	0.309	

f_{mod} [Hz]	x [m]	dis-persion	V [/]	legend
0.1	0.3	P_1	0.880	
		P_2	0.875	
	0.8	P_1	0.710	
		P_2	0.701	

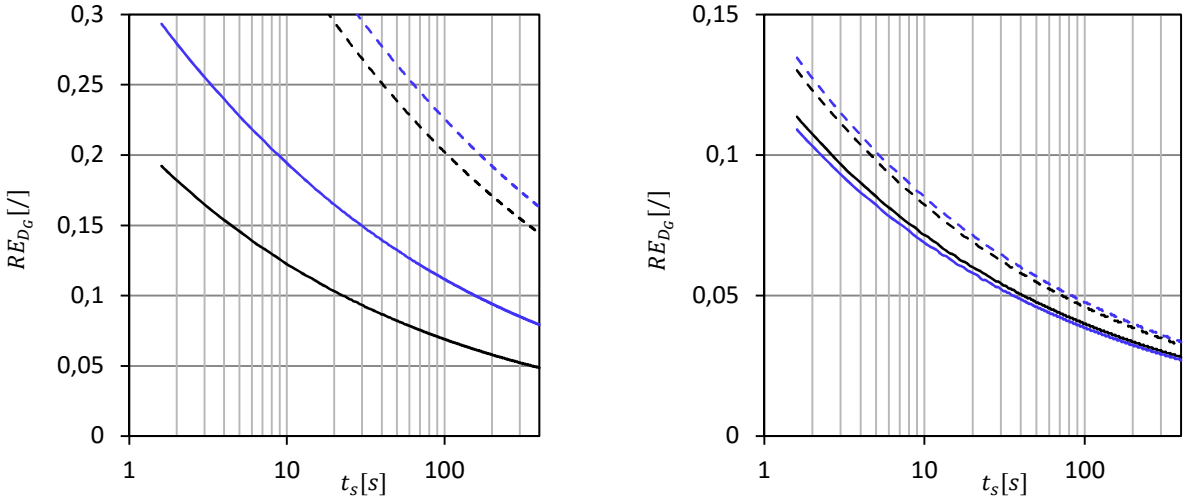

Figure 7: Estimation of relative error ΔD_G depending on averaging time t_s of photon count events, axial measurement position x, compared for $f_{mod} = 0.3Hz$ (left) and $f_{mod} = 0.1Hz$ (right).

Besides the dispersion parameters, RE_{D_G} reflects the amplitude damping sensitivity from measurement height x_1 as well as modulation frequency f_{mod}. Narrow lines symbolize low sensitivity, therefore the maximum tolerable values of RE_{D_G} are lower. The influence by different x significantly increases ΔD_G (due to the higher amplitude damping), changing f_{mod} can reduce RE_{D_G}, drastically as shown by the comparison both graphs, while decreasing sensitivity. Thus, a step by step operation mode can be derived, depending on the knowledge about the present dispersion. For a system with fully unknown dispersion, sensitivity analysis gives measurement conditions for optimum discrimination between dispersion coefficients, resulting in higher RE_{D_G} (or higher t_s) if high dispersion has to be expected. In the next step (or for a system with a more narrow range of expectable dispersion parameters), measurement parameters x and f_{mod} can be adjusted to achieve the best compromise between sensitivity and required t_s. Note that the definition of proper measurement and process parameters is also set by geometric (e.g. adjustable measurement height of the tomographic system, amplitude signal "loss" due to prior amplitude damping below reference position x_1) and device operation limitations (e.g. maximal feasible modulation frequency of the flow controller and lower limit of the sample time of tomographic system). For example for choosing the axial measurement position x_1 for the analysis, not only the amplitude damping prior to x_1 had to be considered, but on the other hand, a minimum distance from the sparger was required to obtain a homogenous

distribution of the gas phase in radial direction. An axial position of $x_1 = 0.15\,m$ was found to represent an adequate measurement position for the initial holdup signal. Aiming for V in the range of $V \in [0.7 \ldots 0.8]$, high sensitivity (see Section 2.2) was only achievable for small axial measurement positions in the range of $x_2 \in [0.22 \ldots 0.50]\,m$ (see Fig. 4). Different modulation frequencies in the corresponding range for high sensitivity of $f \in [0.2 \ldots 0.4]Hz$ were empirically investigated and eventually a modulation frequency of $f_{mod} = 0.318\,Hz$ was found to give high and comparable signal-to-noise-ratio for each measurement height as well as sufficient temporal resolution ($t_s \approx 72s$).

3. Results and discussion

3.1 Data processing

The gas holdup values allocated to one modulation period were fitted with the MatLab® *Curve-Fitting-Toolbox* by the elementary regression model

$$\varepsilon(t) = \bar{\varepsilon} + A \cdot \cos(\omega \cdot t + \phi) = \bar{\varepsilon} + A_\varepsilon \cdot \cos\left(2\pi \frac{n(s)}{n_s} + \phi\right), \tag{24}$$

where $n(s)$ is the index of the current sample in the range of $n(s) \in [1 \dots n_s]$. The coefficient of determination for the regression model R^2 was used for evaluating holdup curves of different runs. Variation of f_{mod} as it was discussed in 2.3, also showed influence on R^2. In consequence only measurements with similar R^2 were used for calculation. Fig. 8 shows an example for experimental data as well as the corresponding regressions at $f_{mod} = 0.318\,Hz$ ($T = 3.145s$). For easier comparison of the periodic shapes, the normalized measurements $\hat{\varepsilon}(t) = \varepsilon(t) - \bar{\varepsilon}$ are shown.

$x'[m]$	$\hat{\varepsilon}(t) = \varepsilon(t) - \bar{\varepsilon}$		$\bar{\varepsilon}$	A	$\Delta\phi\ [s]$	R^2
	experimental	regression				
0.150	■	———	**0.163**	**0.014**	**0.806**	**0.986**
0.225	□	– – – –	0.163	0.012	0.606	0.991
0.300	△	- - - - - -	0.163	0.010	0.428	0.985
0.500	◇	—·—··	0.166	0.007	0.040	0.975

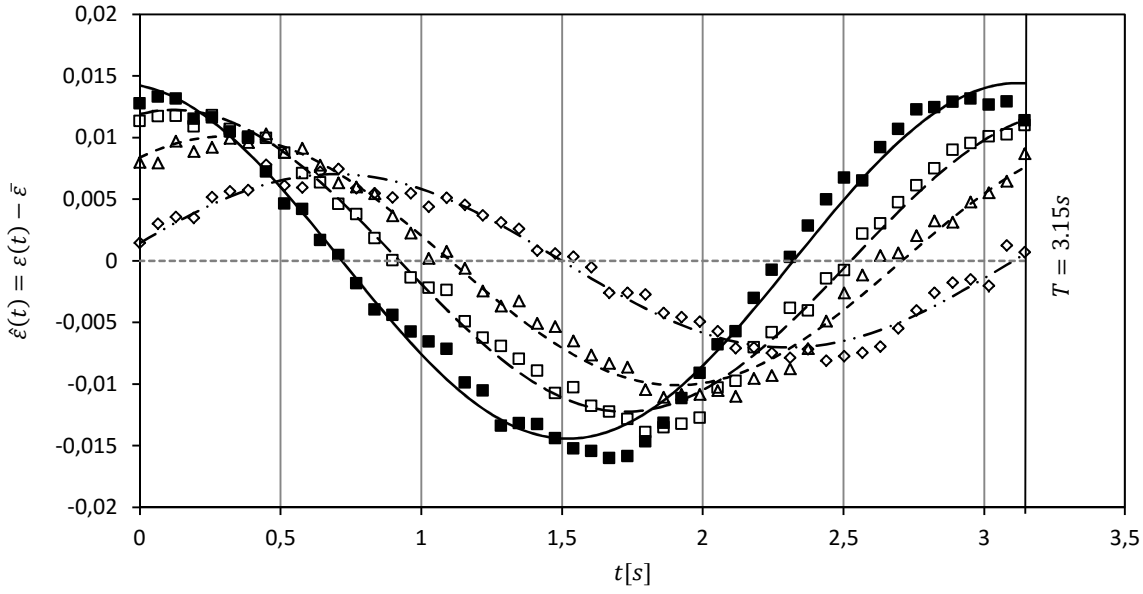

Figure 8: Comparison of normalized holdup data $\hat{\varepsilon}(t)$ (experimental data and regression) obtained at $f_{mod} = 0.318Hz$ ($x_1 = 0.150\,m$ was considered as reference signal for following analysis).

The measured modulation function is in excellent agreement with the sinusoidal modulation induced by the voltage signal generator. Thus, a linear transmission behavior and with it the applicability of the presented calculation model can be confirmed.

3.2 Water / air measurements

The gas holdup was modulated around $\varepsilon = 0.17$ ($u_s = 0.23\, m/s$, see 2.4) with a mean intensity of $A_\varepsilon = 0.01$.

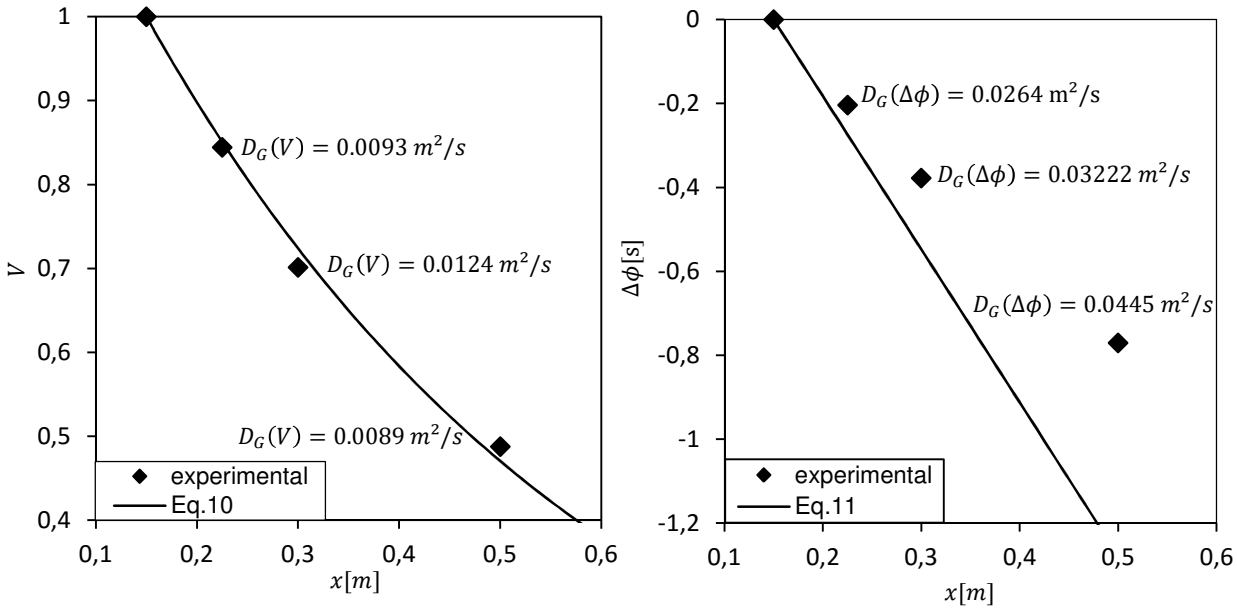

Figure 9: Calculated V and $\Delta\phi$ in comparison with the predictions from Eq. 9 and Eq. 10 for amplitude damping (left) and phase shift (right). Water/air system, $u_S = 0.23\ m/s$, $D_G = 0.0102\ m^2/s$, $f = 0.318\ Hz$, $x_1 = 0.15\ m$.

Averaging of calculated $D_G(V)$ of each measurement position gave $D_G = 0.0102 m^2/s$ which is in good agreement with the mentioned data from literature. According to data of Pilhofer et al. (1978) a dispersion coefficient of $D_G = 0.011\, m^2/s$ was obtained for a bubble rise velocity $u_S = 0.23\, m/s$. For this dispersion value, Eq. 10 and Eq. 11 were used to calculate amplitude damping V and phase shift $\Delta\phi$ respectively (Fig. 9, black lines). While the observed amplitude damping coincides perfectly with the calculated data for all measurement heights, the phase shift deviates for increasing measurement height due to the higher variation of calculated $D_G(\Delta\phi)$ at each measurement position. This can be explained with the (x, f) map in Fig. 4. According to the sensitivity analysis, higher modulation frequencies or measurement distances from the initial measurement height are suggested to reduce total variation of $D_G(\Delta\phi)$ for all measurement positions, which, however, was not feasible with the current setup.

3.3 Glycol / air measurements

To prove applicability of the gas flow modulation method for a higher value of u_s, glycol was used instead of water resulting in $u_s = 0.38\,m/s$ at a lower gas holdup of $\varepsilon = 0.10$. According to Pilhofer et al. (1978), a clearly higher gas dispersion value of $D_G \approx 0.11 m^2/s$ is expected. Calculated $D_G(V)$ resulted in values far beneath the expectations (See Fig. 10, left)

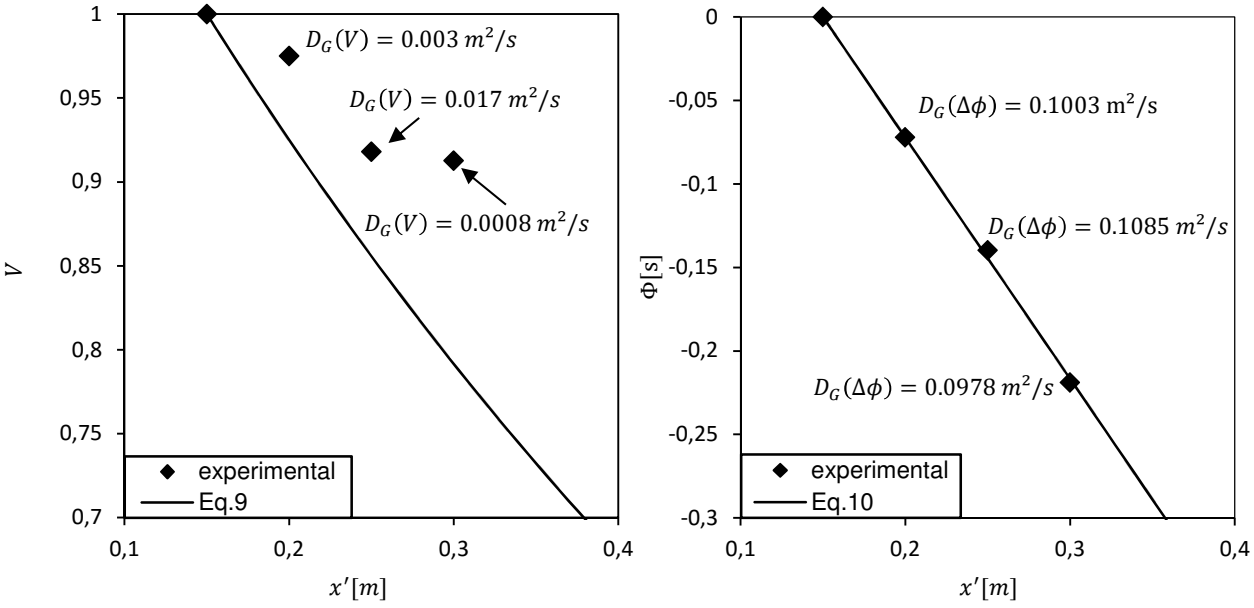

Figure 10: Calculated V and $\Delta\phi$ in comparison with the predictions from Eq. 9 and Eq. 10 for amplitude damping (left) and phase shift (right). Glycol/air system, $u_S = 0.38\,m/s$, $D_G = 0.1022\ m^2/s$, $f = 0.318\,Hz$, $x_1 = 0.15\,m$).

Possible reasons could be the more heterogeneous bubble distribution due to the higher viscosity. Overall shape of detected holdup appeared more blurry than for water data, so that linear transmission behavior could only be considered for measurement positions up to $x = 0.3m$. In contrast to water/air system (section 3.2), averaging of values for all measurement positions gave $D_G(\Delta\phi) = 0.1022\,m^2/s$ which is in good agreement with literature data. Considering the sensitivity analysis, as well as the limited temporal resolution by $n_s = 50$ values of $D_G(\Delta\phi)$ are not recommended for precise analysis of D_G. However the low total variance in Fig. 10 gives reliable information about the range of D_G. From this assumption a detailed analysis for the frequency dependence of $V(D_G)$ was made for estimating proper experimental parameters for amplitude damping analysis (Fig. 11).

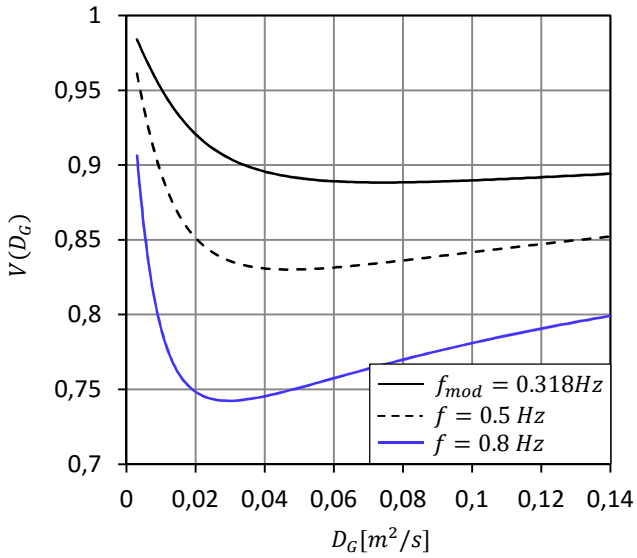

Figure 11: Amplitude damping $V(D_G)$ for increasing modulation frequencies for measured $u_S = 0.38\ m/s$ for measurements between $x_1 = 0.15m$ (ref) and $x_2 = 0.23m$.

Fig. 11 shows prediction of Eq. 9 of values $V(D_G)$ depending on modulation frequency for measurements at $x_1 = 0.15m$ (reference signal) and $x_2 = 0.23m$, whereat the black line indicates the experimental used frequency f_{mod}. The pronounced slope of the line for $V(D_G)$ for $f_{mod} = 0.318\ Hz$ in the range of $D_G < 0.05m^2/s$ indicates a higher measurability with a measurement system of finite accuracy. Measurement of $D_G > 0.06\ m^2/s$ would require highly precise measurement because of the low magnitude in change of $V(D_G)$ at this frequency. Most likely the high variance of $D_G(V)$ of glycol/air measurements (Fig. 10., left) was due to convergence of the iterative solution (Eq. 18) towards lower $D_G(V)$ because the present measurement accuracy insufficient for the case of high dispersion values. In contrast, assuming a higher modulation frequency of $f = 0.8Hz$ (Fig. 11 blue line) indicates a higher slope for large dispersion coefficients and therefore a better measurability. Additionally the sensitivity behavior (section 2.2.) promises still high sensitivity for low x. Obviously the bijective nature of $V(D_G)$ at $f = 0.8Hz$ requires additional effort in the analysis procedure

3.4 Calculated dispersion coefficients

The results of the damped holdup signal analysis were used to calculate the gas phase dispersion coefficients using the introduced equations (Eq. 17, Eq. 18). Multiple measurements were performed in order to improve their accuracy, in particular for reference measurement at x_1, and to confirm high repeatability. All experimental data are included in Fig. 12 together with the data of Pilhofer et al. (1978), for water/air and glycol/air, respectively.

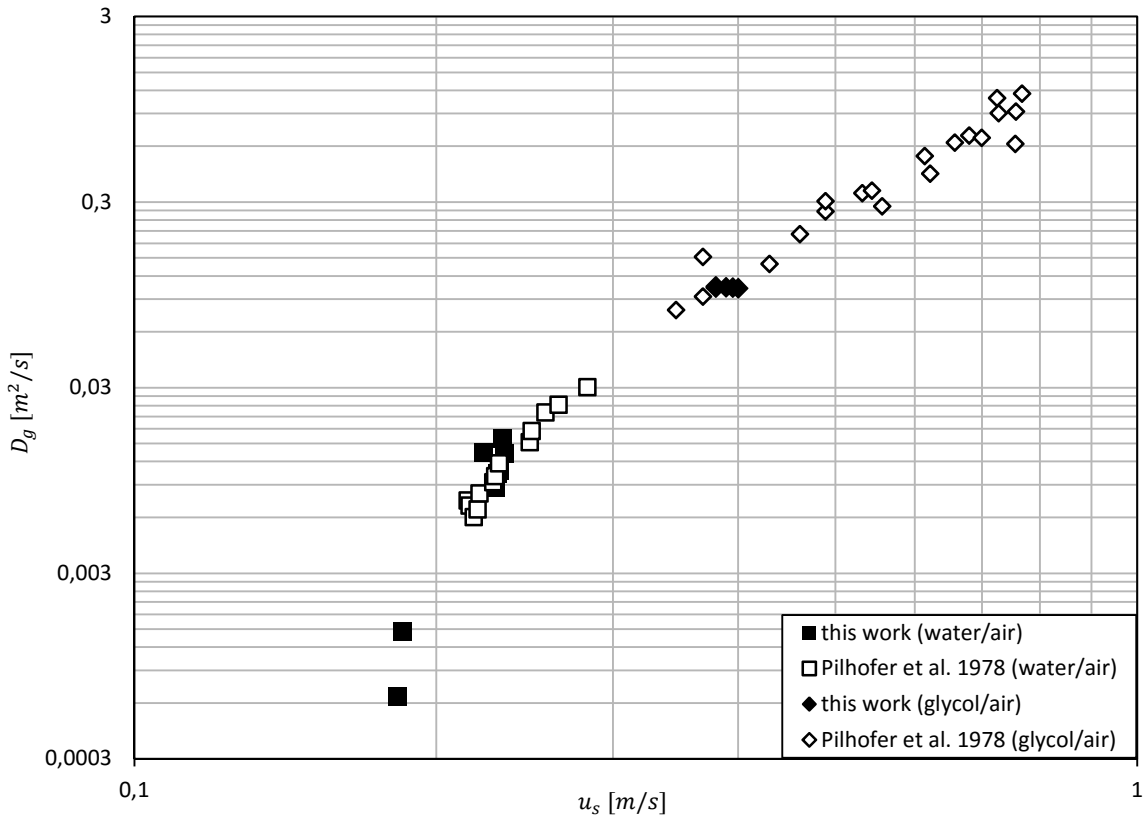

Figure 12: Comparison of the measured D_G with data from Pilhofer et al. (1978) for different bubble swarm velocities u_S.

Water/air measurements as well as glycol/air measurements show an excellent agreement with the literature. Two data points at very low bubble swarm velocity ($u_S = 0.18\,m/s$) were obtained using a sparger configuration with 115 needles of $0.2\,mm$ diameter (not described in Section 2.4), while maintaining a similar holdup value of $\varepsilon \approx 0.10$ at lower $u_G = 0.018\,m/s$. These data even exceed the previous lower limit of available data with respect to bubble swarm velocity and gas dispersion coefficient.

4. Conclusion

In this paper, a new method for the determination of gas phase dispersion coefficients in bubble columns was presented. Thereby, the superficial gas velocity was periodically modulated by a sinusoidal voltage input at the gas phase mass flow controller and the resulting damping and phase shift in gas holdup signals were analyzed. Manipulation on gas dispersion was found to be negligible for low magnitude of gas flow modulation. The new approach is advantageous in terms of non-invasiveness, without any probe sampling and has applicability to various fluids, experimental setups, including industrial settings, due to the detection by gamma-ray densitometry measurement system. Due to the low magnitude of gas flow modulation the resulting low changes in attenuation have to be compensated by long measurement times, ensuring low statistical signal variation. Long term measurements were performed on multiple heights of the column as well as for two different liquids (water, glycol) in semi-batch operating mode using compressed air as gas phase. Dispersion coefficients were calculated from amplitude damping and phase shift with excellent agreement with literature. The new approach bases on the exact solution of the axial dispersion model and allows application under versatile conditions. A sensitivity analysis was performed showing the complex effect that different measurement and process conditions have on amplitude damping and phase shift, which indicates the necessity to adjust the method for different approaches. Thus, optimization of the method is an iterative process combining knowledge of hydrodynamics, process and method properties as well as physical or practical limitations of the measurement system, depending on the particular use case.

5. Nomenclature

A	amplitude (general)	[-]
C	constant	[-]
D	dispersion coefficient	[m²/s]
d	column diameter	[m]
E	extinction	[-]
$E[\lambda]$	expected value of Poisson distribution	[λ]
f	frequency	[Hz]
$\bar{f}$	normalized frequency	[-]
g	gravitational constant	[m/s²]
H	column height	[m]
i	imaginary unit	[-]
j	exponent	[-]
K	constant	[m²/s], [s²/m^4]
k	index variable	[-]
N	number of photon count events	[-]
$\dot{N}$	photon event count rate	[s^{-1}]
n_s	number of sample points	[-]
$n(s)$	number of current sample point	[-]
P	parameter vector	[-]
p	pressure	[bar]
R^2	coefficient of determination (regression)	[-]
RE	relative error (estimated)	[-]
$s[\lambda]$	standard deviation of Poisson distribution	[λ]
T	periodic time	[s]
t	time	[s]
t_s	required time for each sample point	[s]
u_{BS}	slip velocity of largest bubbles	[m/s]
u_i	superficial velocity of phase i	[m/s]
u_S	mean bubble swarm velocity/ bubble rise velocity	[m/s]
u_{LC}	mean circulation velocity of liquid phase	[m/s]
u_R	relative velocity between gas and liquid phase	[m/s]
V	amplitude damping	[-]
x'	height coordinate	[m]
x	measurement distance	[m]
y	variable (Taylor series substitution)	[-]

Greek symbols

Δ	relative error (statistics)	[-]
ε	gas phase holdup	[-]
$\bar{\varepsilon}$	mean void fraction	[-]
$\hat{\varepsilon}$	normalized void fraction	[-]
ζ	drag coefficient	[-]
η	dynamic viscosity	[Pa s]
ϑ	temperature	[°C]
λ	Parameter of Poisson distribution	[λ]
ρ	density	[kg/m³]
ϕ	phase	[rad]
$\Delta\phi$	phase shift	[rad]
ω	angular frequency	[s^{-1}]

Subscripts

0	initial, default
A	modulation amplitude
B	Bach's holdup correlation
c	critical
cal	*calculated*
D_G	dispersion coefficient
ES	exact solution
G	gas phase
GL	two phase / aerated liquid
i	phase index (general)
L	liquid phase
M	Mangartz' correlation
max	maximum
mod	modulation
TS	Taylor series
V	amplitude damping
ε	referring to gas holdup

Abbreviations

ADM	Axial Dispersion Model
CMC	Carboxymethyl Cellulose

CT Computer Tomography

FRA Frequency Response Analysis

RTD Residence Time Distribution

6. References

Cheremisinoff, N. P.Cherremisinoff, N. P., ed. (1986), *Encyclopedia of Fluid Mechanics*, Vol. 3 Gas Liquid Flow, Gulf Publishing Company, Houston.

Hertwig, K.Martens, L., ed. (2007), *Chemische Verfahrenstechnik / Berechnung, Auslegung und Betrieb chemischer Reaktoren*, Oldenbourg Wissenschaftsverlag.

deHaan, A. B. (2015), *Process Technology*, De Gruyter, Berlin/Boston.

Schlüter, S.; Steiff, A. & Weinspach, P.-M. (1992), 'Modeling and simulation of bubble column reactors', *Chemical Engineering and Processing: Process Intensification* **31**(2), 97 - 117.

Levenspiel, O. (1998), *Chemical Reaction Engineering, 3rd Edition*, Wiley.

Shah, Y. T.; Kelkar, B. G. & Godbole, S. P. (2004), 'Design Parameters Estimations for Bubble Column Reactors', *AIChE Journal* **28**(3).

Turner, J. R. & Mills, P. L. (1990), 'Comparison of axial dispersion and mixing cell models for design and simulation of fischer-tropsch slurry bubble column reactors', *Chemical Engineering Science* **45**(8), 2317 - 2324.

Fogler, H. S. (2005), *Elements of Chemical Reaction Engineering (4th Edition)*, Prentice Hall.

Degaleesan, S.; Roy, S.; Kumar, S. B. & Dudukovic, M. P. (1967), 'Liquid Mixing Based on Convection and Turbulent Dispersion in Bubble Columns', *Chemical Engineering Science* **51**(10), 1967 - 1996.

Nauman, E. B. (2002), *Chemical Reactor Design, Optimization, and Scaleup*, McGraw-Hill.

Davis, M. E. & Robert, D. J. (2003), *Fundamentals of chemical reaction engineering*, McGraw-Hill Higher Education.

Deckwer, W. D. (1977), 'Absorption and reaction of isobutene in sulfuric acid', *Chemical Engineering Science* **32**(1), 51 - 57.

Stern, D.; Bell, A. T. & Heinemann, H. (1985), 'Experimental and theoretical studies of Fischer-Tropsch synthesis over ruthenium in a bubble-column reactor', *Chemical Engineering Science* **40**(10), 1917 - 1924.

Behin, J. & Shojaeimehr, T. (2013), 'Modeling of Multistage Bubble Column Reactors for Oxidation Reaction', *Chemical Engineering & Technology* **36**(5), 819-828.

Mangartz, K.-H. (1977), 'Theoretische und experimentelle Darstellung der Funktion einer Blasensäule unter Einbeziehung von axialer Durchmischung und Stoffübergang', PhD thesis, Technische Universität München.

Groen, J. S.; Oldeman, R. G. C.; Mudde, R. F. & van den Akker, H. E. A. (1996), 'Coherent Structure and axial Dispersion in Bubble Column Reactors', *Chemical Engineering Science* **51**(10), 2511 2520.

Rubio., F. C.; Miron, A. S.; Garcia, M. C. C.; Camacho, F. G.; Grima, E. M. & Christi, Y. (2004), 'Mixing in bubble columns: a new approach for characterizing dispersion coefficients', *Chemical Engineering Science* **58**, 4369 - 437.

Zahradnik, J. & Fialova, M. (1996), 'The Effect of Bubbling Regime on gas and liquid phase mixing in Bubble Column Reactors', *Chemical Engineering Science* **51**(10), 2491 - 2500.

Deckwer, W.-D.; Burckhart, R. & Zoll, G. (1974), 'Mixing and mass transfer in tall bubble columns', *Chemical Engineering Science* **29**(11), 2177 - 2188.

Shah, Y. T. & Stiegel, G. J. (1978), 'Backmixing in Gas-Liquid Reactors', *AIChE Journal* **24**(3), 369 - 400.

DeMaria, F. & White, R. R. (1960), 'Transient response study of gas flowing through irrigated packing', *AIChE Journal* **6**(3), 473-481.

Diboun, M. & Schügerl, K. (1967), 'Eine Blasensäule mit Gleichstrom von Wasser und Luft - Mischungsvorgänge in der Gasphase', *Chemical Engineering Science* **22**(2), 147 - 160.

Kago, T.; Sasaki, Y.; Kondo, T. & andY. Kato, S. M. (1989), 'Dispersion of Gas and Liquid in Bubble Columns of Homogeneous Bubble Flow Regime', *Chemical Engineering Communications* **75**(1), 23-38.

Kawagoe, M. & Otake, T. (1989), 'Gas-Phase Mixing in Bubble Columns', *Journal of Chemical Engineering of Japan* **22**(2), 136-142.

Shetty, S. A.; Kantak, M. V. & Kelkar, B. G. (1992), 'Gas-phase backmixing in bubble-column reactors', *AIChE Journal* **38**(7), 1013-1026.

Kantak, M. V.; Hesketh, R. P. & Kelkar, B. G. (1995), 'Effect of gas and liquid properties on gas phase dispersion in bubble columns', *The Chemical Engineering Journal and the Biochemical Engineering Journal* **59**(2), 91 - 100.

Carleton, A. J.; Flain, R. J.; Rennie, J. & Valentin, F. H. H. (1967), 'Some properties of a packed bubble column', *Chemical Engineering Science* **22**(12), 1839 - 1845.

Men'shchikov, V. A. & Aerov, M. E. (1967), 'Longitudinal Mixing of Gas phase in Bubble-plate Reactors', *Theor. Found. Chem. Eng.*.

S.Wachi, Y. N. (1990), 'Gas-phase dispersion in bubble columns', *Chemical Engineering Science* **45**(4), 901 - 905.

Towell, G. D. & Ackerman, G. H. (1972), 'Axial Mixing of Liquid and Gas in Large Bubble Reactors', *Chemical Reaction engineering*.

Koelbel, H.; Langemann, H. & Platz, J. (1962), 'Eigenschaften des Blasensäulen-Reaktors - Das Verweilzeitspektrum der gasförmigen Phase', *Dechema Monograph*(41), 225 - 243.

Joseph, S.; Shah, Y. T. & Kelkar, B. G. (1984), 'A Simple Experimental Techniquie to Measure Gas Phase Dispersion in Bubble Columns', *Chemical Engineering Communications* **28**(4-6), 223-230.

Seher, A. & Schumacher, V. (1978), 'Verweilzeitmessung von Flüssigkeits- und Gasphase in großsen Blasensäulen mit radioaktiven Indikatoren', *Chemie Ingenieur Technik* **50**(12), 967.

Field, R. W. & Davidson, J. F. (1980), 'Axial Dispersion in Bubble Columns', *Transactions of the Institution of Chemical Engineers* **85**(4), 228 - 236.

Mangartz, K.-H. & Pilhofer, T. (1980), 'Untersuchungen zur Gasphasendispersion in Blasensäuleneaktoren', *Verfahrenstechnik 14* **14**, 40 ff..

Gray, R. I. & Prados, J. W. (1963), 'The Dynamics of a Packed Gas Absorber by Frequency Response Analysis', *AIChE Journal* **9**(2), 211 - 216.

Kramers, H. & Alberda, G. (1953), 'Frequency Response Analysis of Continuous Flow Systems', *Chemical Enginnering Science* **2**, 173 - 181.

W.Böxkes, H. H. (1972), 'Vor- und Nachteile verschiedener Befragungstechniken zur Analyse des Mischverhaltens in chemischen Reaktoren', *Chemie Ingenieur Technik* **44**(14).

Gray, R. I. (1961), 'The Dynamics of a Packed Gas Absorber by Frequency Response Analysis', PhD thesis, The Graduate Council of The University of Tennessee.

Coulon, G. (1971), 'Untersuchungen des Stoffaustauschs in einer Blasensäule', *Chemie Ingenieur Technik* **43**, 280 -285.

Vermeer, D. J. & Krishna, R. (1981), 'Hydrodynamics and mass transfer in bubble columns in operating in the churn-turbulent regime', *Industrial & Engineering Chemistry Process Design and Development* **20**(3), 475-482.

Kraume, M. & Zehner, P. (1989), 'Modellierung der Fluiddynamik in Blasensäulen', *Chemie Ingenieur Technik* **61**(4), 332-333.

P.Zehner, G. S. (1984), 'Konzept zur Beschreibung der Vermischung der Gasphase in Blasensäulen', *Chemie Ingenieur Technik* **56**(12), 934-935.

Pilhofer, T.; Bach, H. F. & Mangartz, K. H. (1978), 'Determination of Fluid Dynamic Parameters in Bubble Column Design', *ACS symposium series* **65**, 372-383.

Joshi, J. B. (1982), 'Gas phase dispersion in bubble columns', *The Chemical Engineering Journal* **24**(2), 213 - 216.

Heijnen, J. J. & Riet, K. V. (1984), 'Mass transfer, mixing and heat transfer phenomena in low viscosity bubble column reactors', *The Chemical Engineering Journal* **28**(2), B21 - B42.

Hampel, U. (2015), 'Anordnung und Verfahren zur Dispersionsmessung sowie Mehrphasenapparat mit einer solchen Anordnung'(DE 10 2014 118 649 B3 2015.12.24).

Deckwer, W. D.Dialer, K.; Pawlowski, J. & Springe, W., ed. (1985), *Grundlagen der chemischen Technik - Reaktionstechnik in Blasensäulen*, Otto Salle Verlag, Verlag Sauerländer.

Bach, H. F. & Pilhofer, T. (1977), 'Einflußs verschiedener Stoff - und Betriebsgrößsen auf den relativen Gasgehalt in Blasensäulen', *Chemie Ingenieur Technik* **49**(5), 435.

Azizi, S.; Yadav, A. & M. Lau S. R. M., S. (2016), 'ICMF 2016 International Conference on Multiphase Flow Firenze, Italy,"Gas and Liquid Dynamics in Bubble Columns: Advanced Flow Imaging with Ultrafast X-Ray and Radiocative Particle Tracking'.

Hampel, U.; Bieberle, A.; Hoppe, D.; Kronenberg, J.; Schleicher, E.; Sühnel, T.; Zimmermann, F. & Zippe, C. (2007), 'High resolution gamma ray tomography scanner for flow measurement and non-destructive testing applications', *Review of Scientific Instruments* **78**(10), 103704.

Bieberle, A.; Kronenberg, J.; Schleicher, E. & Hampel, U. (2007), 'Design of a high-resolution gamma-ray detector module for tomography applications', *Nuclear Instruments and Methods in Physics Research Section A: Accelerators, Spectrometers, Detectors and Associated Equipment* **572**(2), 668 - 675.

Leon, M. A.; Maas, R. J.; Bieberle, A.; Schubert, M.; Nijhus, T. A.; der. Schaaf, J.; Hampel, U. & Schouten, J. C. (2013), 'Hydrodynamics and gas-liquid mass transfer in a horizontal rotating foam stirrer reactor', *Chemical Engineering J* **217**, 10 - 21.

Tschentscher, R.; Schubert, M. & Schouten, A. B. T. A. N. J. S. U. H. J. C. (2013), 'Gas Holdup of Rotating Foam Reactors Measured by Gamma-Tomography - Effect of Solid Foam Pore Size and Liquid Viscosity', *AIC* **59**(1), 146 - 154.

Bieberle, A.; Härting, H.-U.; S-Rabha; Schubert, M. & Hampel, U. (2013), 'Gamma-Ray Computed Tomography for Imaging of Multiphase Flows', *Chemie Ingenieur Technik* **85**(7), 1002 - 1011.

Härting, H.; Bieberle, A. & Schubert, R. L. F. L. M. (2015), 'Hydrodynamics of co-current two-phase flow in an inclined rotating tubular fixed bed reactor - Wetting

intermittency via periodic catalyst immersion', *Chemical Engineering Science* **128**, 147 - 158.

Rollbusch, P.; Becker, M.; Ludwig, M.; Bieberle, A.; Grünewald, M.; Hampel, U. & Franke, R. (2015), 'Experimental investigation of the influence of column scale, gas density and liquid properties on gas holdup in bubble columns', *International Journal of Multiphase Flow* **75**, 88-106.

M.Neumann, T. S. & A.Bieberle, U. H. (2016), 'An Experimental Study on the Gas Entrainment in Horizontally and Vertically Installed Centrifugal Pumps', *Journal of Fluids Engineering* **138**(9), 091301-091301.

A. Bieberle, J. S.; A. Spies, G. S. & W. Kühnel, U. H. (2015), 'Hydrodynamics analysis in micro-channels of a viscous coupling using gamma-ray computed tomography', *Flow Measurement and Instrumentation* **45**, 288 - 297.